Journal of Engineering Issues and Solutions

Effect of Opening Location and Size on the In-Plane Lateral Performance of Unreinforced Masonry Walls: A Zone-Based Numerical Study

Bed Prakash Gupta[1*], Bibekananda Mandal[2*]

[1] Department of Civil Engineering, Everest Engineering College, Pokhara University, Kathmandu, Nepal
[2] Department of Civil Engineering, National Institute of Technology Rourkela, Rourkela, India,
*Corresponding author: mandalb@nitrkl.ac.in, bedprakashgupta04@gmail.com

Received: May 12, 2026; Revised: 13 June, 2026; Accepted: July 11, 2026

Abstract

Unreinforced masonry (URM) walls with openings exhibit complex in-plane lateral behavior that is governed not only by the size of the opening but also by its longitudinal and vertical position within the wall. Despite this, most existing studies characterize the structural impact of openings solely through the Total Perforation Ratio, without accounting for the positional sensitivity of the opening relative to the internal diagonal load path. This study presents a numerical parametric investigation into the effect of opening location and size on the in-plane lateral performance of URM walls using a Simplified Micro-Modeling framework implemented in ABAQUS. The wall length was discretized into three longitudinal zones: Zone I (loaded side), Zone II (central), and Zone III (passive side); and openings of three area sizes (3.70%, 6.17%, and 8.64%) with corresponding aspect ratios of 0.85, 1.41, and 1.97 were systematically positioned at multiple vertical locations within each zone, yielding twenty-three perforated wall models. Lateral strength, initial stiffness, and failure pattern were evaluated relative to a solid wall reference model. Results demonstrate that Zone II produces the most severe strength reductions, reaching 51.56% for mid-elevation openings that directly sever the diagonal compressive strut. Bottom-positioned openings in Zone III prove equally critical, with reductions reaching 57.22% due to elimination of the strut anchor at the passive corner. Initial stiffness degrades monotonically with increasing opening area, with maximum reductions of 33.54%, 36.13%, and 31.59% in Zones I, II, and III, respectively. The failure mechanism varies systematically from diagonal tension to rocking-dominated toe crushing as opening size increases and location shifts toward the passive side.

Keywords: *Unreinforced masonry, Simplified micro-modeling, In-plane lateral loading, Zone sensitivity, Opening location, Diagonal tension failure, Toe crushing*

1 Introduction

Unreinforced masonry (URM) remains a fundamental construction method used across the world due to its historical reliability [Hendry,1998]. While these structures are highly effective at supporting vertical gravity loads, they present a significant challenge for structural analysis. This complexity arises because masonry is a composite material that is both heterogeneous and anisotropic; its mechanical response is dictated by the intricate bond between individual units and mortar joints [Lourenco,1996]. Because of this, forecasting how a masonry wall will behave under lateral pressures; such as those from seismic activity or wind; is exceptionally difficult. To bypass the high expenses and technical difficulties of large-scale laboratory testing, researchers now rely on Finite Element Modeling (FEM) [Lotfi & Shing,1994]. This numerical approach offers a precise and cost-effective way to simulate the structural performance of masonry under various loading conditions [Lourenco,1996; Lotfi & Shing,1994].

Conventional structural evaluations frequently rely on the Equivalent Frame Method (EFM) to analyze masonry walls with openings [Mangenes & Fontana,1998]. This approach simplifies a complex, solid wall by representing it as a skeletal frame composed of vertical members (piers) and horizontal members (spandrels) linked by rigid, non-deformable nodes [Kappos et al.,2002]. The primary advantage of EFM is its computational speed, as it reduces a 3D continuum into a 1D frame of interconnected line elements [Belmouden & Lestuzzi,2009]. By assuming that the deformation and energy dissipation are concentrated within these piers and spandrels, engineers can quickly estimate the global lateral response of a building [Kappos et al.,2002; Lagomarsino et al.,2013].

However, this simplification comes with significant accuracy trade-offs. As emphasized by Lourenço [Lourence,1996], the nonlinear behavior of masonry is deeply influenced by the exact shape and location of window or door openings. The EFM often struggles to account for the complex stress concentrations that develop at the corners of these voids, where cracks typically initiate [Parisi & Augenti,2013]. Furthermore, most standard codes rely on the Total Perforation Ratio, the simple percentage of the wall area that is hollow-to predict strength loss. This global metric is often misleading; it cannot account for the localized stress shifts that occur when openings are shifted asymmetrically or placed in different longitudinal regions of the wall [Howlader,2019: Vasconcelos & Lourenco,2009]. While two walls might have the same total opening area, their actual failure modes and load paths can be completely different depending on whether the openings are located near the loading point or at the distal end of the wall [Parisi & Augenti,2013]. This positional sensitivity of openings, which the total perforation ratio entirely ignores, constitutes the primary motivation for the present study.

Recent progress in Finite Element Analysis (FEA), particularly through software like ABAQUS, has enabled researchers to examine masonry failure with high precision using the Concrete Damaged Plasticity (CDP) model and discrete interface elements. Historically, the most precise method is Detailed Micro-Modeling (DMM), where bricks, mortar, and the bond between them are modeled as individual components with their own material laws [Abdulla et al.,2017]. While DMM accurately captures the thickness of mortar and its nonlinear behavior, it is computationally expensive. The processing power required for such detail often limits its use to small laboratory samples rather than full-scale walls with multiple openings, making it impractical for the large-scale parametric studies required to understand zonal sensitivity [D'Altri et al.,2020; Reccia et al.,2018].

At the other end of the spectrum is Macro-Modeling, which treats the entire wall as a single, homogenous block. While this method is very fast and easy to compute, it often overlooks the fine details of how cracks propagate through specific joints [Lourenco,1996]. To resolve these issues, the Simplified Micro-Modeling (SMM) approach was developed as an ideal intermediate strategy [Lourenco & Rots,1997]. By expanding the bricks to include the thickness of the mortar and replacing the physical joints with zero-thickness interface elements, SMM significantly reduces computational time while maintaining the accuracy of a micro-scale analysis [Abdulla et al.,2017; Macorini & Izzuddin,2011].

In SMM framework adopted in the present study, the initiation of damage at the brick mortar interface is governed by a quadratic stress criterion, which defines the onset of irreversible degradation as a function of the normalized normal and shear traction components acting simultaneously on the cohesive interface [Abdulla et al.,2017; Camanho,2002]. This criterion enables the model to simulate both tensile debonding (Mode I) and frictional sliding (Mode II) failure mechanisms within a single unified framework, which is essential for accurately reproducing the mixed-mode fracture behavior observed at mortar joints in unreinforced masonry walls subjected to in-plane lateral loading [Lourenco & Rots,1997]. The subsequent damage evolution is governed by a fracture energy based law, ensuring that the post-peak softening response of the interface is physically consistent with experimentally measured fracture properties of the brick-mortar bond [Benzeggagh & Kenane,1996].

Despite the efficiency and accuracy of the SMM framework, its application in existing literature has largely been limited to studying the total size of openings or the aspect ratio (AR) of the resulting masonry piers on the global lateral response of masonry walls [Howlader,2019: Abdulla et al.,2017: Doran et al.,2023]. Most current research assumes that the impact of a window or door is purely a function of the Perforation Ratio, regardless of where that opening is located along the length of the wall [Vasconcelos & Lourenco,2009; Sajid et al.,2018; Noor,2021]. However, this global assumption overlooks a critical structural reality: the path of the internal compression strut is highly sensitive to the longitudinal position of a void [Sajid et al.,2018].

In this study, the SMM framework is employed to conduct a systematic numerical parametric investigation into the effect of opening location and size on the in-plane lateral performance of unreinforced masonry walls, moving beyond the conventional area based characterization of opening influence. The wall length is discretized into three equal longitudinal zones, and openings of different area and height to width ratios are systematically positioned at multiple vertical locations within each zone. This zonal classification allows for a rigorous quantification of how the longitudinal and vertical position of an opening relative to the diagonal compression strut path governs the reduction in lateral strength and initial stiffness of the wall.

2 Numerical Analysis

2.1 Interface Modeling: Surface-Based Cohesive Behavior

In SMM framework, the fracture behavior of mortar joints is captured using a cohesive based surface model, which idealizes the head and bed joints as traction-separation interfaces [Camanho,2002]. It is governed by three stages namely; linear-elastic traction separation stage, damage-initiation stage, and damage-evolution stage [Park & Paulino,2011].

The initial elastic response of the cohesive interface is defined by a stiffness matrix that relates the nominal tractions (t) to the displacement separations (δ) across the interface. In this stage, the traction–separation relationship is assumed to be linear, representing the elastic behavior of the interface prior to damage initiation [Lourenco & Rots,1997]. This linear elastic relationship can be expressed in Eq. 1 in the form of an elastic stiffness matrix, which mathematically describes the proportional relationship between the interface tractions and the corresponding separations.

$$t = \begin{Bmatrix} t_n \\ t_s \\ t_t \end{Bmatrix} = \begin{bmatrix} K_{nn} & 0 & 0 \\ 0 & K_{ss} & 0 \\ 0 & 0 & K_{tt} \end{bmatrix} \begin{Bmatrix} \delta_n \\ \delta_s \\ \delta_t \end{Bmatrix} = [K]\{\delta\} \qquad (1)$$

Where, K is elastic stiffness matrix, t is nominal traction vector and δ is corresponding traction separation vector. For the SMM approach, the interface between the expanded fictitious units must be assigned an equivalent stiffness representing the mechanical behavior of the mortar joint [Lourenco & Rots,1997]. This equivalent stiffness in Eq. 2 & 3 is used to simulate the joint interface response and can be expressed as follows:

$$K_{nn} = \frac{E_u E_m}{h_m(E_u - E_m)} \qquad (2)$$

$$K_{ss} \text{ and } K_{tt} = \frac{G_u G_m}{h_m(G_u - G_m)} \qquad (3)$$

Where *Eu* is Young's modulus of brick units, *Em* is the Young's modulus of mortar units, *hm* in the thickness of mortar (mm), *Gu* is shear modulus of brick units and *Em* is shear modulus of mortar units. The adjusted modulus of elasticity (*Eadj*) for the expanded masonry units must be determined to accurately represent the elastic response of the original masonry assemblage, which consists of both masonry units and mortar joints. This calculation considers the overall geometry of the masonry assembly as well as the elastic moduli of the brick units and the mortar. By assuming a uniform distribution of stresses within the masonry components and perfect bonding between the units and mortar, the adjusted modulus of elasticity can be expressed using Eq. 4 [11, 14].

$$E_{adj} = \frac{H E_u E_m}{n h_u E_m + (n-1) h_m E_u} \qquad (4)$$

To represent the coupled interaction between tensile damage and shear sliding, a quadratic stress criterion was adopted to define the onset of damage initiation [Abdulla et al.,2017, Camanho,2002]. This criterion is governed by user-defined tensile and shear strength parameters specified in the damage initiation section while defining the interaction property in ABAQUS. Damage initiation occurs when the quadratic stress criterion of the normalized contact stresses reaches unity, which can be expressed as shown in Eq. 5.

$$\left\{\frac{t_n}{t_n^{max}}\right\}^2 + \left\{\frac{t_s}{t_s^{max}}\right\}^2 + \left\{\frac{t_t}{t_t^{max}}\right\}^2 = 1 \qquad (5)$$

Once the damage initiation stage is reached, damage evolution stage starts with propagation of cracks in the masonry joints that causes stiffness degradation resulting in strength loss and failure of joints [Park & Paulino,2011]. The Benzeggagh & Kenane(1996) law provides a method to calculate the total critical fracture energy (G_{TC}) when an interface fails under a combination of tension (Mode I) and shear (Mode II and Mode III) forces shown in Eq. 6. Using a power-law relationship, the law interpolates between the pure mode I, mode II and mode III fracture energies based on an exponent value and for this analysis this exponent (η) is taken as 2. The tensile fracture energy rate is calculated based on study by [Lotfi & Shing,1994] and shear fracture energy rate is taken as per [Lourenco,1996].

$$G_{TC} = G_{IC} + (G_{IIC} - G_{IC})\left\{\frac{G_{II} + G_{III}}{G_I + G_{II} + G_{III}}\right\}^{\eta} \qquad (6)$$

2.2 Material Constitutive model: Concrete Damaged Plasticity (CDP)

The inelastic behavior of the expanded masonry units was governed by the CDP model, which assumes that the two main failure mechanisms are tensile cracking and compressive crushing [Lubliner et al.,1989]. The inelastic behavior of the expanded masonry units is characterized using the CDP model. This model captures the distinct mechanical responses of masonry under tension and compression by implementing specific stress-strain relations and stiffness degradation variables. Following the relations suggested by [Zhang et al.,2017], the compressive stress (σ_c) and tensile stress (σ_t) of the masonry can be formulated by Eq. 7 & 8.

$$\frac{\sigma_c}{f_{cm}} = \frac{h}{1 + (h-1)(\varepsilon/\varepsilon_{cm})^{h/(h-1)}} \frac{\varepsilon}{\varepsilon_{cm}} \tag{7}$$

$$\frac{\sigma_t}{f_{tm}} = \begin{cases} \varepsilon/\varepsilon_{tm} & , \quad \varepsilon/\varepsilon_{tm} \le 1 \\ \dfrac{\varepsilon/\varepsilon_{tm}}{2(\varepsilon/\varepsilon_{tm} - 1)^{1.7} + \varepsilon/\varepsilon_{tm}}, & \quad \varepsilon/\varepsilon_{tm} > 1 \end{cases} \tag{8}$$

Where f_{cm} and f_{tm} represent the compressive and tensile strengths of masonry, while and ε_{cm} and ε_{tm} denote the corresponding peak strains in compression and tension. The compression factor h, which governs the form of the compressive stress-strain curve is set as 1.633 by default [Zhang et al.,2017, Kaushik et al.,2007].

Under the combined stresses, the masonry units undergo stiffness degradation which is quantified by a scalar damage variable (d) given in Eq. 9. The evolution of damage in either compression or tension is dependent on the stress (σ), the corresponding strain (ε), and the initial elastic modulus (E), expressed as [Lubliner et al.,1989]:

$$d = 1 - \sqrt{\frac{\sigma}{E_o \varepsilon}} \tag{9}$$

This damage variable is integrated into the CDP model to simulate the progressive reduction in elastic stiffness matrix as cracking or crushing progresses [D'Altri et al.,2020, Zhang et al.,2017].

2.3 Description of FE model

A three-dimensional finite element model of the masonry wall was developed in ABAQUS using solid elements. Specifically, 8-node linear brick elements with reduced integration and enhanced hourglass control (C3D8R) were adopted, as they provide improved numerical stability, convergence, and computational efficiency. An experimentally tested masonry shear wall with dimensions of 990 mm in length, 1000 mm in height, and 100 mm in thickness was considered (Figure 1). The wall consisted of 18 brick layers, where each brick had dimensions of 210 mm × 52 mm × 100 mm (length × height × width). The mortar joint thickness was 10 mm, and the mortar was composed of cement, lime, and sand in a ratio of 1:2:9. The masonry units were arranged in a stretcher bond pattern [Vermeltfoort et al.,1993].

In SMM approach, the brick units were expanded in both the longitudinal and vertical directions to account for the mortar joint thickness. Consequently, expanded brick units with dimensions of 220 mm × 62 mm × 100 mm were used in the model, while the mortar joints were represented as zero-thickness interfaces. The mechanical properties of the brick units, mortar, and expanded masonry units are summarized in Table 1. The nonlinear behavior of the masonry units under both compression and tension was modeled using the CDP model available in ABAQUS. Furthermore, a surface-based cohesive interaction was defined between the faces of the expanded units to simulate the mechanical behavior of the mortar joints.

The top layer of the masonry wall was connected to a steel beam measuring 990 mm × 70 mm × 100 mm in length, height, and thickness, respectively. This steel beam served as a rigid loading plate to distribute both vertical pre-compression and lateral displacement uniformly across the top surface of wall. For the application of boundary conditions and loading, three reference points were defined within the model. The first reference point (RP1) was located at the top of the steel beam and was used to apply top boundary conditions, the second reference point (RP2) was located at the base of the wall and was used to enforce base boundary condition (encastre), and the third reference point (RP3) was located at the left edge of the top brick layer and was used to apply lateral displacement. Each reference point was coupled to its corresponding surface through kinematic constraint, ensuring full transfer of the applied loads and boundary conditions to the masonry assembly (Figure 3). A uniform vertical compression stress of 0.3 MPa was applied on the top face of steel beam as pre-compression load and in second load step, a monotonically increasing lateral displacement of 4 mm was applied in the in-plane horizontal direction through RP3 (Figure 4). The global element seed size of 30 mm was adopted for the expanded brick units based on the mesh sensitivity study conducted by Abdulla et al. [Abdulla et al.,2017]. To investigate the spatial sensitivity of openings, the wall length was divided into three equal longitudinal segments, designated as Zone I, Zone II, and Zone III (Figure 2).

Table 1: Mechanical and material properties of the masonry components adopted in the SMM numerical model.

Type of Characteristics	Categories	Characteristics	Values	Units
Linear Characteristics	Brick units	*Eu*	16700 [Abdulla et al.,2017]	MPa
	Mortar units	*Em*	780 [Abdulla et al.,2017]	MPa
	Expanded units	*Eadj*	5000 [Eq. 4]	MPa
	Poisson ratio	Υ	0.15 [Lourenco & Rots et al.,1997]	
	Interface	*Knn*	81 [Eq. 2]	N/mm^3
		Kss & Ktt	35.57 [Eq. 3]	N/mm^3
Non-Linear Joint Interface	Cohesion	C	0.35 [Abdulla et al., 2017]	MPa
	Friction coef.	μ	0.75 [Abdulla et al.,2017]	
	Tensile strength		0.25 [Abdulla et al.,2017]	MPa
	Tensile damage energy	G_{IC}	0.0019 [Lotfi & Shing, 1994]	N/mm
	Shear damage energy	G_{IIC}	0.0312 [Lourenco,1996]	N/mm
Concrete damage plasticity	Dilation angle	φ	30^O [default]	
	Eccentricity		0.1[default]	
	fbo/fco		1.16 [default]	
	K		0.67 [default]	
	Viscocity parameter		0.0001 [Abdulla et al.,2017]	
Compressive strength of assembly			10.5 [Abdulla et al.,2017]	MPa
Tensile Strength of assembly			2 [Abdulla et al.,2017]	MPa

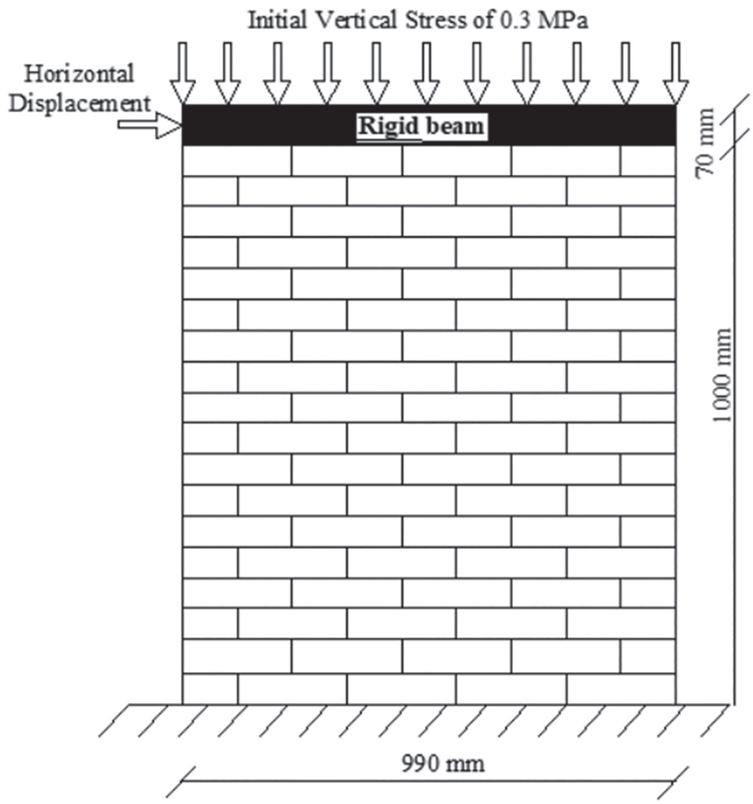

Figure 1: Test setup of masonry shear wall

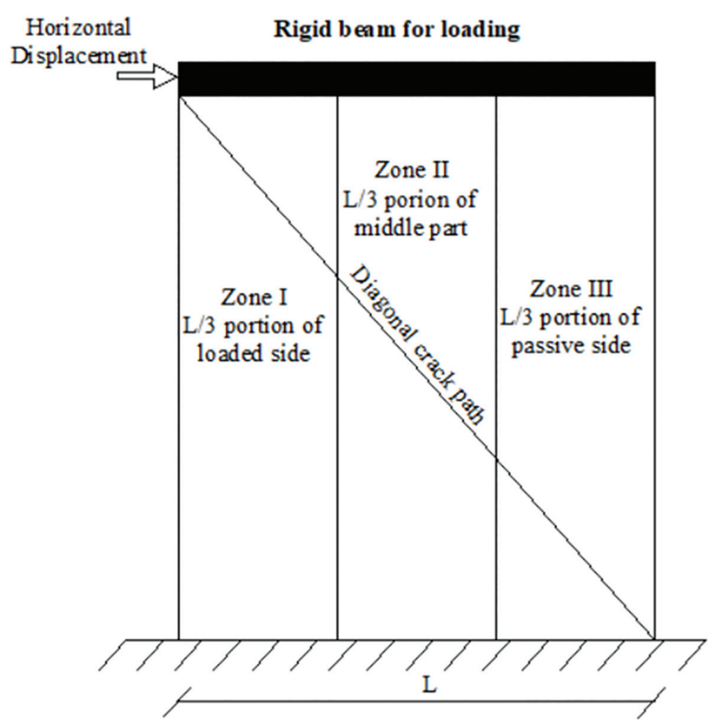

Figure 2: Zone definition

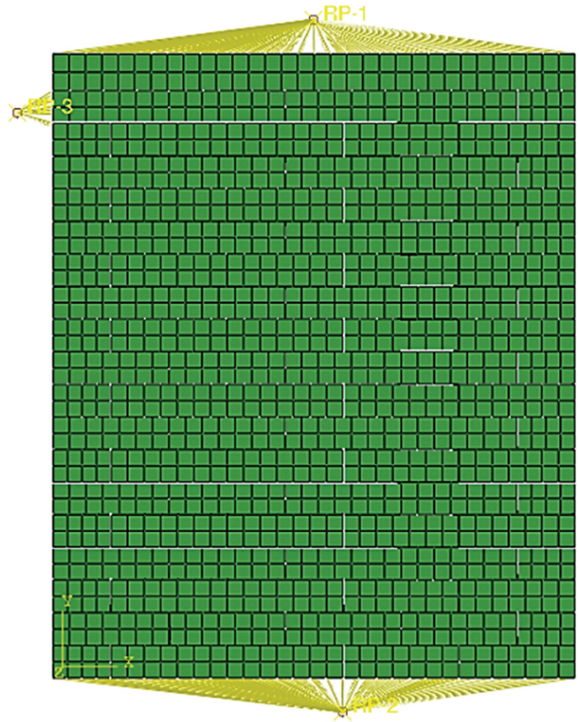

Figure 3: Numerical model of masonry wall in ABAQUS showing kinematic coupling constraints between reference points (RP-1, RP-2, and RP-3) and their associated surfaces

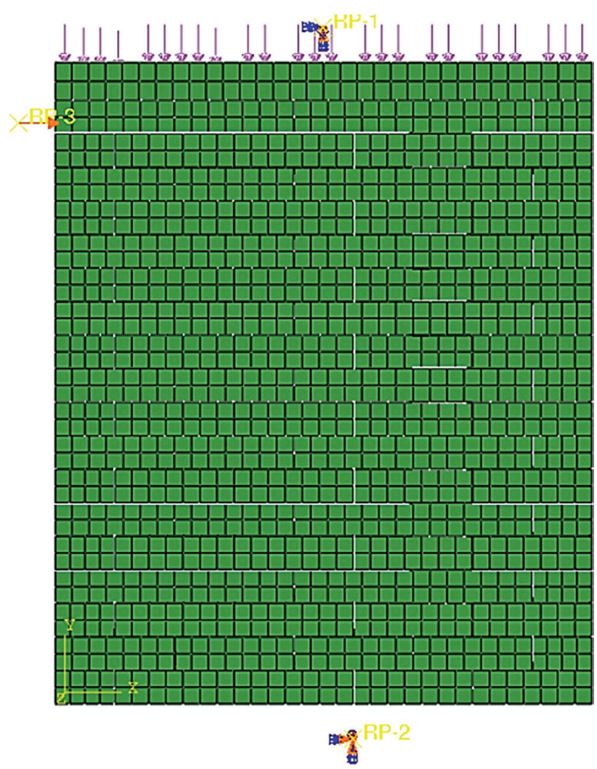

Figure 4: Numerical model showing loading and boundary conditions

3 Validation of Numerical Model

The experimentally tested masonry shear wall with the same dimensions described in the previous section was also used for validation of the numerical model [Vermeltfoort et al.,1993]. The comparison between the experimental and numerical results is presented in terms of the failure pattern and the force–displacement response, as shown in Figure 5 and Figure 6.

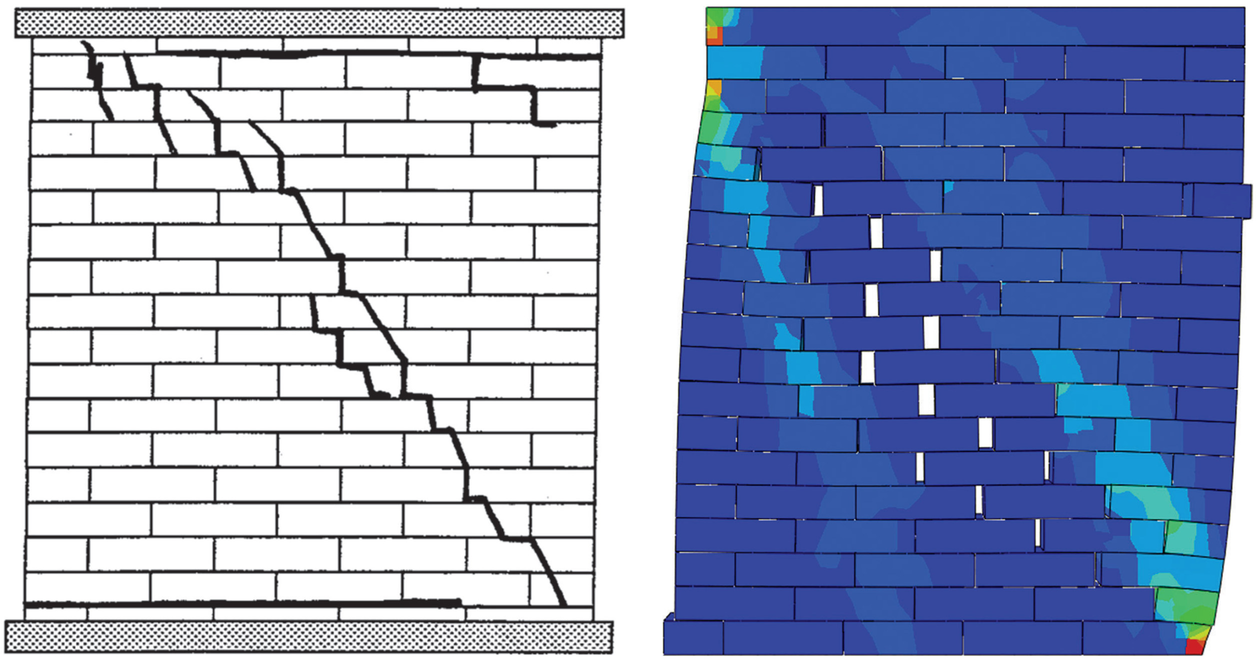

(a) (b)

Figure 5: Comparison of failure patterns of the solid wall reference model; (a) experimentally observed diagonal tension crack pattern [Vermeltfoort et al.,1993]; (b) numerically predicted damage pattern with a deformation scale factor of 20

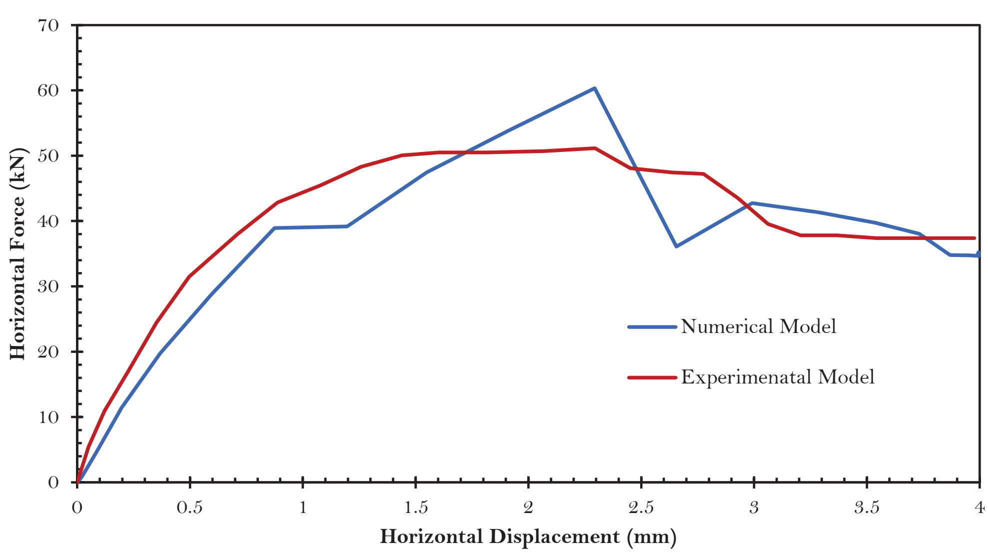

Figure 6: Comparison of pushover curve for experimental and numerical results

The numerical model predicted a peak lateral load of 59.93 kN against the experimental value of 51.05 kN, corresponding to a difference of 17.4%. The displacement at peak load was 2.3 mm for both curves, indicating exact agreement in deformation capacity. The normalized root mean square error (RMSE) computed over the full loading range of 0–4 mm was 9.70%, confirming good overall agreement between the two force-displacement curves.

The overestimation of peak load is primarily attributed to the idealization inherent in the SMM framework. The numerical model assumes perfectly bonded interfaces and geometrically regular brick-mortar joints throughout the wall, whereas the physical specimen inevitably contains pre-existing micro-cracks, material variability, and workmanship imperfections that reduce the actual load-carrying capacity below the numerically predicted value. A peak load discrepancy in the range of 10-20% is widely reported in comparable SMM validation studies [Abdulla et al.,2017; Lourenco & Rots,1997].

The fluctuations observed in the post-peak region of the numerical curve are a known numerical characteristic of the damage-plasticity framework and do not represent physical instability [Lubliner et al.,1989]. They arise because when a cohesive interface element reaches its damage threshold, it undergoes a sudden stiffness drop, releasing stored elastic energy abruptly [Lotfi & Shing,1994; Camanho,2002]. The model then redistributes this energy through the remaining undamaged elements, causing temporary local load drops and recoveries that appear as oscillations in the curve [Dassault Systemes, 2014; Lubliner,1989].

4 Results & Discussion

The numerical parametric study was carried out on 24 URM numerical models alongside a solid reference wall with different opening percentage of 3.70%, 6.17%, and 8.64% having corresponding height-to-width aspect ratios (AR) of 0.85, 1.41, and 1.97 respectively. Further, these openings were placed at three zones (Zone I: loaded side; Zone II: middle; Zone III: passive side) with varying vertical positions within each zone to evaluate structural response. Results are discussed with explicit reference to the diagonal tension failure pattern of the solid wall, whose principal crack propagates from the top-loaded corner toward the bottom-passive corner, traversing Zone II at mid-to-lower elevations and terminating in the lower portion of Zone III.

4.1 Effect on Lateral In-Plane Strength

4.1.1 Zone I: Loaded Side

Zone I encompasses openings located on the loaded side of the wall (horizontal location ratio HLR ≤ 0.33), where the diagonal compressive strut originates. For the smallest opening size (area = 3.70%, AR = 0.85), the decrease in lateral strength ranges from 11.92% to 35.75% depending on the vertical position of the opening. The upper bound of 35.75% corresponds to the top-positioned opening, which intercepts the strut near its origin at the load application point, while the lower bound of 11.92% corresponds to the bottom-positioned opening, which lies below the principal strut trajectory and therefore causes minimal disruption to load transfer. For the medium opening size (area = 6.17%, AR = 1.41), the range of strength decrease widens from 26.25% to 44.20%, reflecting the amplified disruption caused by the larger void at positions that partially intersect the strut. For the largest opening size (area = 8.64%, AR = 1.97), the strength decrease ranges from 22.97% to 31.42% (Figure 7). The narrowing of this range with increasing opening size in Zone I suggests that the larger opening, when placed at the top, may partially redistribute the strut around the void due to the availability of adequate masonry material on both sides of the opening, thereby moderating the peak strength loss relative to the medium-size case (Table 2).

Overall, Zone I strength reductions remain moderate and are predominantly governed by vertical position rather than opening area alone. The consistent finding that bottom-positioned openings in Zone I are the least detrimental provides a practical design guidance: when openings in the loaded zone are unavoidable, placing them at lower elevations minimizes the impact on lateral capacity.

4.1.2 Zone II: Middle Zone

Zone II represents the middle longitudinal segment of the wall and, based on the failure pattern of the solid wall, corresponds directly to the region through which the diagonal compressive strut passes. Openings in this zone therefore have the potential to sever the primary internal load path, making Zone II the most structurally sensitive region identified in this study.

For the smallest opening size (area = 3.70%, AR = 0.85), the strength decrease ranges from 30.46% to 51.56%, with the upper bound corresponding to the mid-elevation position that most directly intersects the diagonal crack path. For the medium opening size (area = 6.17%, AR = 1.41), the range of strength decrease is 12.40% to 28.72%. While the upper bound is comparatively lower than the 3.70% case, this may reflect differences in the specific vertical alignment of the medium opening relative to the crack path centerline, wherein the medium opening at the top of Zone II is positioned above the critical strut region and thus produces less disruption. For the largest opening size (area = 8.64%, AR = 1.97), the strength decrease ranges from 30.17% to 36.70%, with the narrower range indicating that the large void consistently intersects the diagonal strut regardless of vertical position, producing a more uniform degradation across elevations (Figure 8).

The results for Zone II collectively confirm that openings at mid-to-lower elevations within the central zone of the wall represent the most adverse configuration for lateral strength, with reductions exceeding 50% in the most critical cases. This finding directly challenges the conventional reliance on the Total Perforation Ratio as the sole predictor of strength loss, as two walls with identical perforation ratios but different zone placements can exhibit dramatically different structural responses.

4.1.3 Zone III: Passive Side

Zone III encompasses openings on the passive (non-loaded) side of the wall, where the diagonal compressive strut terminates near the lower corner. For the smallest opening size (area = 3.70%, AR = 0.85), the strength decrease ranges from 12.77% to 57.22%. The lower bound of 12.77% corresponds to upper-positioned openings that are located above the crack terminus and therefore exert limited influence on the strut, while the upper bound of 57.22% represents the most severe strength reduction observed across all zones for this opening size (Figure 9). This extreme value at the bottom of Zone III arises because the opening is placed at the precise location where the diagonal strut anchors, eliminating the residual load-bearing capacity of the strut's terminal zone.

For the medium opening size (area = 6.17%, AR = 1.41), the strength decrease ranges from 22.18% to 53.49%, and for the largest opening (area = 8.64%, AR = 1.97), from 27.50% to 49.75%. In all cases, the bottom-positioned openings in Zone III consistently produce the highest strength reductions, confirming that the lower passive corner is a structurally critical region that should be kept free of openings whenever possible.

4.2 Effect on Initial Lateral Stiffness

4.2.1 Zone I: Loaded Side

In Zone I, the percentage decrease in initial stiffness increases progressively with opening area. For the 3.70% opening and AR of 0.85, the average stiffness reduction is 14.10%; for the 6.17% opening with AR of 1.41, this increases to 21.74%; and for the 8.64% opening and AR of 1.97, the reduction reaches 33.54% (Figure 7). The consistent upward trend confirms that larger openings in the loaded zone remove proportionally more of the cross-sectional stiffness contribution, even when placed in positions that produce modest strength reductions. The stiffness reductions in Zone I are the lowest across all zones for corresponding opening sizes, which is consistent with the position of Zone I away from the diagonal strut's primary stiffness-governing region.

4.2.2 Zone II: Middle Zone

Zone II exhibits stiffness reductions of 19.88%, 23.88%, and 36.13% for opening areas of 3.70%, 6.17%, and 8.64%, respectively (Figure 8). The increase from Zone I to Zone II stiffness reductions for comparable opening sizes reflects the additional disruption to the elastic load path caused by openings located along the diagonal strut.

4.2.3 Zone III: Passive Side

In Zone III, stiffness reductions of 18.86%, 26.91%, and 31.59% are recorded for opening areas of 3.70%, 6.17%, and 8.64%, respectively (Figure 9). These values are intermediate between Zones I and II for the smallest opening size but exceed Zone II reductions for the medium opening, suggesting that Zone III becomes progressively more sensitive to stiffness degradation as opening size increases.

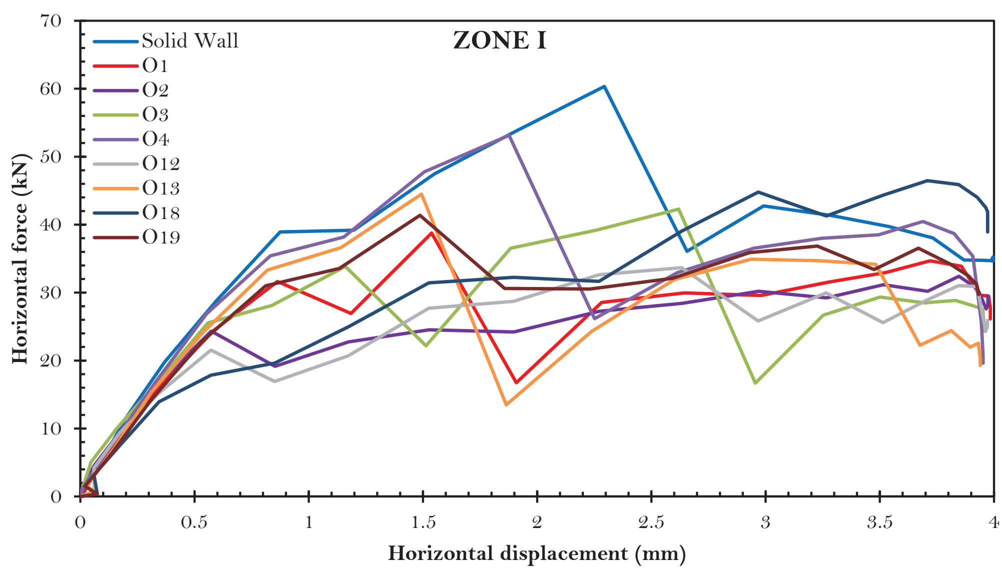

Figure 7: Lateral load–displacement curves for Zone I opening configurations: comparison of wall models with varying opening area percentages and height-to-width aspect ratios under monotonic in-plane lateral loading

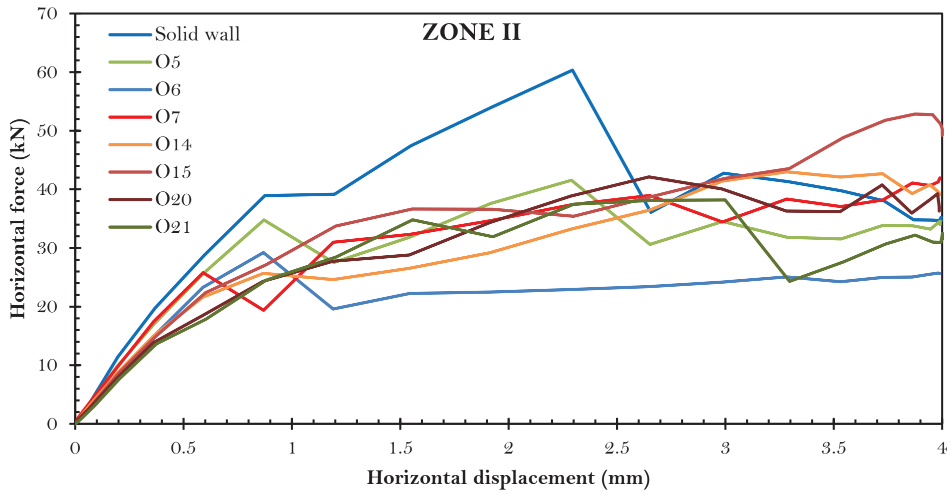

Figure 8: Lateral load–displacement curves for Zone II opening configurations: comparison of wall models with varying opening area percentages and height-to-width aspect ratios under monotonic in-plane lateral loading

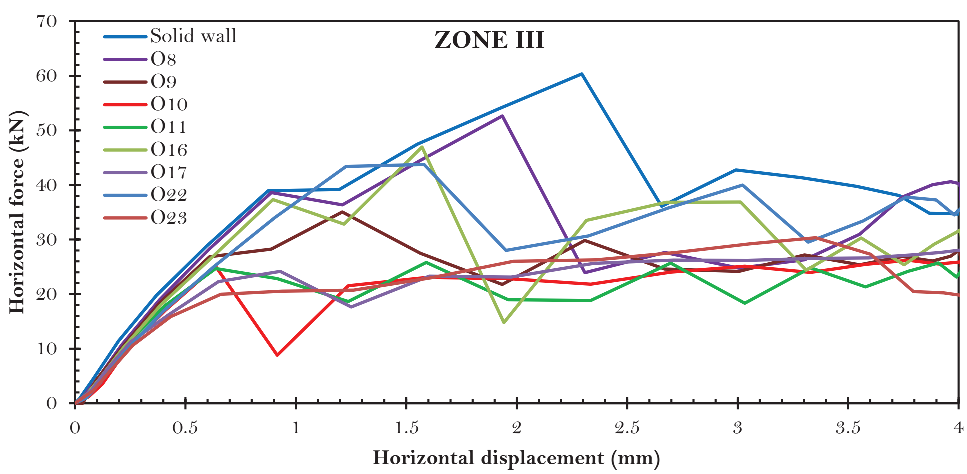

Figure 9: Lateral load–displacement curves for Zone III opening configurations: comparison of wall models with varying opening area percentages and height-to-width aspect ratios under monotonic in-plane lateral loading

4.3 Effect on failure mode

4.3.1 Zone I: loaded side

Small openings permit partial re-formation of the of the diagonal compressive strut around the void, and the resulting failure pattern retains the characteristics of diagonal tension broadly consistent with the solid wall reference. As the opening area (OA) increases within Zone I, the diagonal crack is progressively suppressed and the failure mode transitions toward rocking-dominated behaviour, evidenced by the concentration of tensile damage at the loaded corner and a largely undamaged wall body with intense stress localisation at the compression toe (Figure 10).

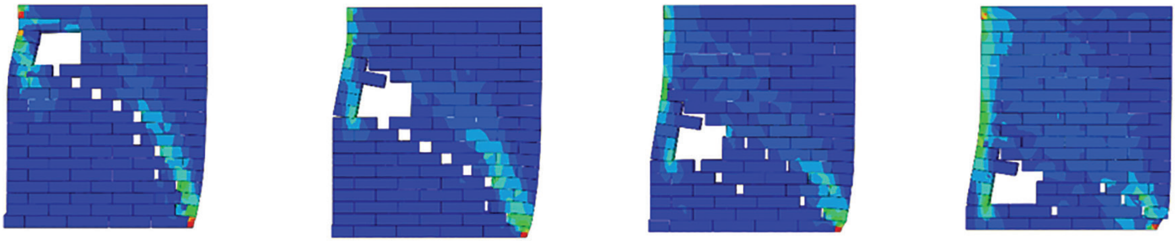

(a) OA=3.7%, AR=0.85 (b) OA=3.7%, AR=0.85 (c) OA=3.7%, AR=0.85 (d) OA=3.7%, AR=0.85

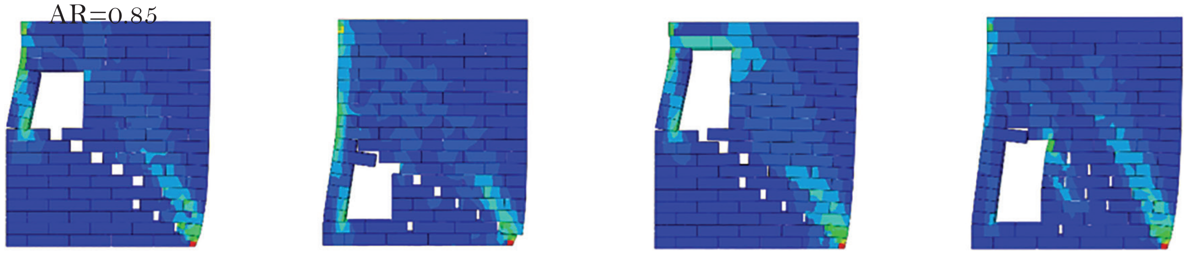

(e) OA=6.17%, AR=1.41 (f) OA=6.17%, AR=1.41 (g) OA=8.64%, AR=1.97 (h) OA=8.64%, AR=1.97

Figure 10: Failure patterns of masonry wall models with openings in Zone I for varying opening area (OA) percentages and height-to-width aspect ratios (AR) at different locations under monotonic in-plane lateral loading (scale factor = 20).

4.3.2 Zone II: Middle zone

The presence of an opening directly along the diagonal strut path disrupts the internal force transfer at its most critical cross-section. For the smallest opening size, the diagonal crack is visibly deflected around the opening while partial strut continuity is maintained. For medium and large openings in Zone II, the strut is fully severed, and the failure pattern transitions to localised joint damage adjacent to the opening perimeter with no coherent diagonal crack propagating through the wall body, indicating a shift from shear-dominated to flexure-dominated failure (Figure 11).

4.3.3 Zone III: Passive side

The transition from diagonal tension to toe-crushing rocking failure is most pronounced for larger openings at the bottom of the zone, where elimination of the compression strut anchor forces rigid-body rotation of the wall about the passive corner. This rocking behaviour is characterised in the ABAQUS contour plots by an essentially undamaged wall body shown in blue with intense compressive damage concentrated at the bottom-right corner, which is entirely consistent with the toe-crushing failure observed in the attached numerical results (Figure 12).

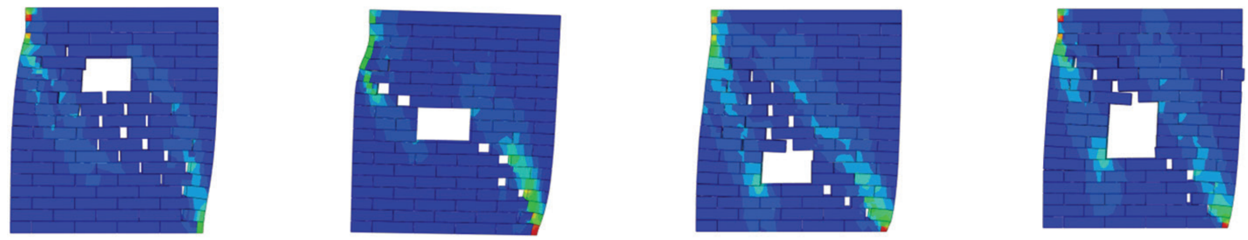

(a) OA=3.7%, AR=0.85 (b) OA=3.7%, AR=0.85 (c) OA=3.7%, AR=0.85 (d) OA=6.17%, AR=1.41

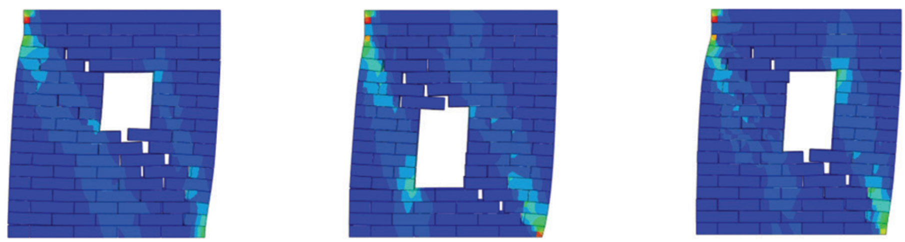

(e) OA=6.17%, AR=1.41 (f) OA=8.64%, AR=1.97 (g) OA=8.64%, AR=1.97

Figure 11: Failure patterns of masonry wall models with openings in Zone II for varying opening area (OA) percentages and height-to-width aspect ratios (AR) at different locations under monotonic in-plane lateral loading (scale factor = 20).

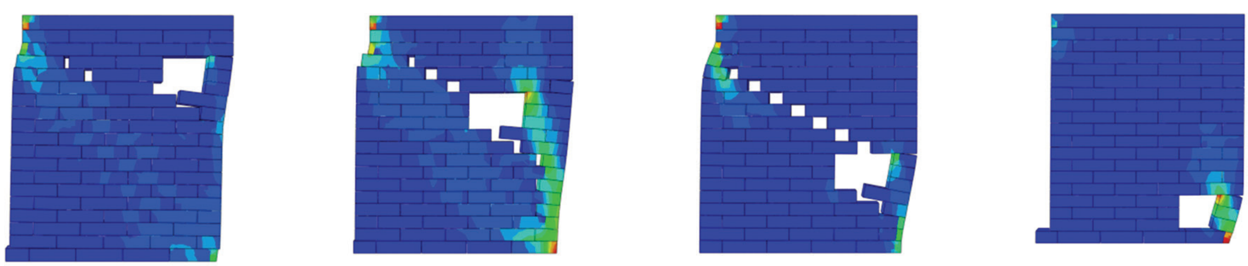

(a) OA=3.7%, AR=0.85 (b) OA=3.7%, AR=0.85 (c) OA=3.7%, AR=0.85 (d) OA=3.7%, AR=0.85

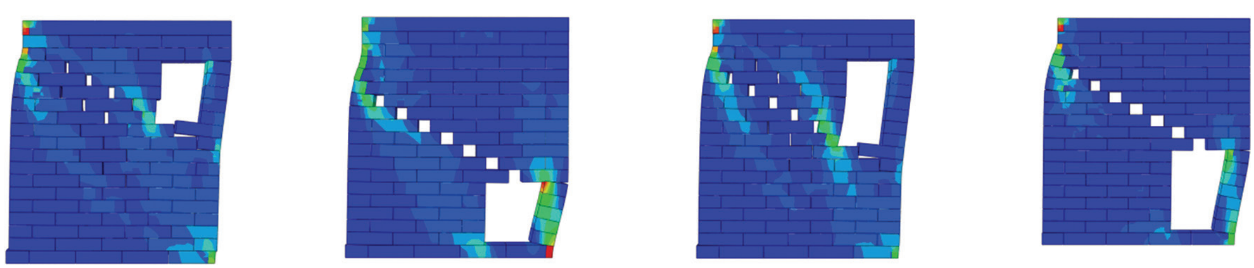

(e) OA=6.17%, AR=1.41 (f) OA=6.17%, AR=1.41 (g) OA=8.64%, AR=1.97 (h) OA=8.64%, AR=1.97

Figure 12: Failure patterns of masonry wall models with openings in Zone III for varying opening area (OA) percentages and height-to-width aspect ratios (AR) at different locations under monotonic in-plane lateral loading (scale factor = 20).

4.4 Synthesis and Comparative Discussion

Considering both strength and stiffness responses together, three principal observations emerge from parametric study. First, Zone II is the most critical longitudinal position for lateral strength, as openings in this zone directly intersect the diagonal compressive strut and can reduce strength by more than 50% in the most severe cases. Second, Zone III bottom positions are equally critical for strength despite being on the passive side, as they disrupt the strut terminus and produce the highest individual strength reductions in the dataset (Table 2). Finally, a systematic transition from diagonal tension to rocking dominated toe crushing failure is observed as opening size increases and location shifts toward the passive side, producing higher displacement capacity but substantially reduced lateral strength.

Table 2: Summary of structural performance parameters for all masonry wall models

Zone	Model	Opening Area (%)	Ht. to width ratio	Size of opening Width (mm)	Height (mm)	Max. shear force (kN)	Percentage decrease in strength	Initial stiffness (kN/mm)	Percentage decrease in initial stiffness
	Solid wall					60.33		49.97	
I	O1	3.7	0.85	220	961	38.77	35.74	42.93	14.10
	O2	3.7		220	713	32.40	46.29	43.77	12.41
	O3	3.7		220	465	42.29	29.91	46.42	7.12
	O4	3.7		220	217	53.14	11.92	49.03	1.88
	O12	6.17	1.41	220	775	33.66	44.20	39.11	21.74
	O13	6.17		220	279	44.49	26.25	45.37	9.21
	O18	8.64	1.97	220	837	46.47	22.97	33.21	33.54
	O19	8.64		220	279	41.38	31.42	43.07	13.81
II	O5	3.7	0.85	440	837	41.55	31.13	44.39	11.16
	O6	3.7		440	589	29.23	51.56	40.04	19.88
	O7	3.7		440	341	41.96	30.46	44.97	10.00
	O14	6.17	1.41	440	527	43.00	28.72	38.04	23.88
	O15	6.17		550	713	52.85	12.40	38.19	23.57
	O20	8.64	1.97	440	465	42.13	30.17	33.38	33.21
	O21	8.64		550	651	38.19	36.70	31.92	36.13
III	O8	3.7	0.85	770	899	52.63	12.77	47.61	4.73
	O9	3.7		660	713	35.05	41.91	45.49	8.96
	O10	3.7		770	403	26.20	56.58	40.55	18.86
	O11	3.7		770	155	25.81	57.22	41.27	17.41
	O16	6.17	1.41	770	837	46.95	22.18	44.42	11.10
	O17	6.17		770	217	28.06	53.49	36.52	26.91
	O22	8.64	1.97	770	775	43.74	27.50	40.90	18.15
	O23	8.64		770	279	30.32	49.75	34.18	31.59

5 Conclusions

This study presents a numerical parametric investigation into the effect of opening location and size on the in-plane lateral performance of unreinforced masonry walls, using a SMM framework implemented in ABAQUS. Twenty-three perforated wall models with openings of three area sizes (3.70%, 6.17%, and 8.64%) placed at three longitudinal zones and multiple vertical positions were analyzed under monotonic lateral displacement. The following conclusions are drawn:

- Zone II, the middle longitudinal zone of the wall, is the most critical placement region for lateral in-plane strength. Openings located in this zone directly intersect the principal diagonal compressive strut, regardless of their size, and produce the most severe reductions in lateral load-carrying capacity among all zones examined.
- The bottom position of Zone III, on the passive side of the wall, is equally critical to Zone II and should be treated as such in seismic vulnerability assessments. This severity arises because the lower passive corner serves as the termination zone of the diagonal compressive strut, and the introduction of an opening at this location eliminates the residual load-bearing capacity of the strut anchor. Among all configurations examined, bottom-positioned openings in Zone III consistently produced the highest individual reductions in lateral strength across all opening sizes investigated.
- Within Zone I on the loaded side, the vertical position of the opening exerts a strong and decisive influence on structural performance. Top-positioned openings, which intercept the diagonal strut near its point of origin at the load application zone, are significantly more detrimental than bottom-positioned openings, which lie below the principal strut trajectory and therefore cause comparatively minor disruption to the internal load path.
- Initial lateral stiffness degrades progressively with increasing opening area across all three zones, following a consistent and monotonic trend irrespective of the horizontal or vertical position of the opening. Unlike lateral strength, which is strongly governed by the location of the opening relative to the diagonal crack path, stiffness degradation is predominantly controlled by the total quantity of material removed from the wall cross-section. This distinction is of practical importance: the stiffness of a perforated wall cannot be reliably estimated from location-based considerations alone, and the opening area must be explicitly accounted for in lateral stiffness modelling of unreinforced masonry structures.
- The failure mode transitions systematically from diagonal tension to rocking dominated toe crushing as opening size increases and location shifts from the loaded side toward the passive corner, as discussed in section 4.3.
- The results collectively demonstrate that the structural impact of an opening in an unreinforced masonry wall is governed by three interdependent parameters acting simultaneously; the longitudinal zone of placement relative to the diagonal crack path, the vertical position of the opening within that zone, and the overall size of the opening. No single parameter in isolation is sufficient to characterize or predict the reduction in lateral performance.

The present study is subject to the following limitations, which define the scope of future work: (i) all analyses were conducted under monotonic lateral loading; the response under cyclic or earthquake-type loading may differ due to stiffness and strength degradation effects not captured in the present framework; (ii) only single rectangular openings were considered, walls with multiple openings or non-rectangular voids may exhibit different zonal sensitivity patterns; (iii) the wall geometry was fixed at a single aspect ratio of 990 mm × 1000 mm and the zonal boundaries may shift for walls of different proportions.

Author contributions B.G. played a role in, Methodology, Analysis, Validation, Writing—Original Draft, Editing, Visualization, and Data Curation. B.M. provided Conceptualization, Supervision, Writing—Review & Editing. All authors read and approved the final manuscript.

References

Hendry, A. W. (1998). *Structural masonry.* Macmillan Education UK. http://dx.doi.org/10.1007/978-1-349-14827-1

Lourenço, P. J. B. B. (1996). *Computational strategies for masonry structures.* Delft University Press.

Lotfi, H. R., & Shing, P. B. (1994). Interface model applied to fracture of masonry structures. *Journal of Structural Engineering, 120*(1), 63–80. https://doi.org/10.1061/(ASCE)0733-9445(1994)120:1(63)

Magenes, G., & Fontana, A. (1998). Simplified non-linear seismic analysis of masonry buildings. *Proceedings of the British Masonry Society, 8*, 190–195.

Kappos, A., Penelis, G., & Drakopoulos, C. (2002). Evaluation of simplified models for lateral load analysis of unreinforced masonry buildings. *Journal of Structural Engineering, 128*(7), 890. https://doi.org/10.1061/(ASCE)0733-9445(2002)128:7(890)

Belmouden, Y., & Lestuzzi, P. (2009). An equivalent frame model for seismic analysis of masonry and reinforced concrete buildings. *Construction and Building Materials, 23*(1), 40–53. https://doi.org/10.1016/j.conbuildmat.2007.10.023

Lagomarsino, S., Penna, A., Galasco, A., & Cattari, S. (2013). TREMURI program: An equivalent frame model for the nonlinear seismic analysis of masonry buildings. *Engineering Structures, 56*, 1787–1799. https://doi.org/10.1016/j.engstruct.2013.08.002

Parisi, F., & Augenti, N. (2013). Seismic capacity of irregular unreinforced masonry walls with openings. *Earthquake Engineering & Structural Dynamics, 42*(1), 101–121. https://doi.org/10.1002/eqe.2195

Howlader, M. (2019). *In-plane behaviour of perforated unreinforced masonry (URM) walls.*

Vasconcelos, G., & Lourenço, P. B. (2009). Experimental characterization of stone masonry in shear and compression. *Construction and Building Materials, 23*(10), 3337–3345. https://doi.org/10.1016/j.conbuildmat.2009.06.045

Abdulla, K. F., Cunningham, L. S., & Gillie, M. (2017). Simulating masonry wall behaviour using a simplified micro-model approach. *Engineering Structures, 151*, 349–365. https://doi.org/10.1016/j.engstruct.2017.08.021

D'Altri, A. M., de Miranda, S., Castellazzi, G., & Sarhosis, V. (2020). Modeling strategies for the computational analysis of unreinforced masonry structures: Review and classification. *Archives of Computational Methods in Engineering, 27*(4), 1153–1185. https://doi.org/10.1007/S11831-019-09351-X

Reccia, E., Leonetti, L., Trovalusci, P., & Cecchi, A. (2018). A multiscale/multidomain model for the failure analysis of masonry walls: A validation with a combined FEM/DEM approach. *International Journal for Multiscale Computational Engineering, 16*(4), 325–343. https://doi.org/10.1615/IntJMultCompEng.2018026988

Lourenço, P. B., & Rots, J. G. (1997). Multisurface interface model for analysis of masonry structures. *Journal of Engineering Mechanics, 123*(7), 660–668. https://doi.org/10.1061/(ASCE)0733-9399(1997)123:7(660)

Macorini, L., & Izzuddin, B. A. (2011). A non-linear interface element for 3D mesoscale analysis of brick-masonry structures. *International Journal for Numerical Methods in Engineering, 85*(12), 1584–1608. https://doi.org/10.1002/nme.3046

Camanho, P. P. (2002). Mixed-mode decohesion finite elements for the simulation of delamination in composite materials. *Composite Materials.*

Benzeggagh, M. L., & Kenane, M. (1996). Measurement of mixed-mode delamination fracture toughness of unidirectional glass/epoxy composites with mixed-mode bending apparatus. *Composites Science and Technology, 56*(4), 439–449. https://doi.org/10.1016/0266-3538(96)00005-X

Doran, B., Karslioglu, M., Unsal Aslan, Z., & Vatansever, C. (2023). Experimental and numerical investigation of unreinforced masonry walls with and without opening. *International Journal of Architectural Heritage, 17*(11), 1833–1854. https://doi.org/10.1080/15583058.2022.2080611

Sajid, H. U., Ashraf, M., Ali, Q., & Sajid, S. H. (2018). Effects of vertical stresses and flanges on seismic behavior of unreinforced brick masonry. *Engineering Structures, 155*, 394–409. https://doi.org/10.1016/j.engstruct.2017.11.013

Noor-E-Khuda, S. (2021). An explicit finite-element modeling method for masonry walls using continuum shell element. *Journal of*

Architectural Engineering, *27*(4). https://doi.org/10.1061/(ASCE)AE.19435568.0000518

Park, K., & Paulino, G. H. (2011). Cohesive zone models: A critical review of traction-separation relationships across fracture surfaces. *Applied Mechanics Reviews*, *64*(6). https://doi.org/10.1115/1.4023110

Dassault Systèmes. (2014). *Abaqus analysis user's manual* (Vol. 5). Dassault Systèmes Simulia Corp.

Lubliner, J., Oliver, J., Oller, S., & Oñate, E. (1989). A plastic-damage model for concrete. *International Journal of Solids and Structures*, *25*(3), 299–326. https://doi.org/10.1016/0020-7683(89)90050-4

Zhang, S., Yang, D., Sheng, Y., Garrity, S. W., & Xu, L. (2017). Numerical modelling of FRP-reinforced masonry walls under in-plane seismic loading. *Construction and Building Materials*, *134*, 649–663. https://doi.org/10.1016/j.conbuildmat.2016.12.091

Kaushik, H. B., Rai, D. C., & Jain, S. K. (2007). Stress-strain characteristics of clay brick masonry under uniaxial compression. *Journal of Materials in Civil Engineering*, *19*(9), 728–739. https://doi.org/10.1061/(ASCE)0899-1561(2007)19:9(728)

Vermeltfoort, A. T., Raijmakers, T. M. J., & Janssen, H. J. M. (1993). Shear tests on masonry walls. In *Proceedings of the 6th North American Masonry Conference* (pp. 1183–1193).